Parametric Bragg resonances in waves on a shallow fluid over a periodically drilled bottom

M. Torres,[1] J. P. Adrados,[1] F. R. Montero de Espinosa,[2] D. García-Pablos,[3] and J. Fayos[4]
[1]*Instituto de Física Aplicada, Consejo Superior de Investigaciones Cientificas (CSIC), Serrano 144, 28006 Madrid, Spain*
[2]*Instituto de Acústica, Consejo Superior de Investigaciones Cientificas (CSIC), Serrano 144, 28006 Madrid, Spain*
[3]*Laboratorio de Física de Sistemas Pequeños y Nanotecnologia, Consejo Superior de Investigaciones Cientificas (CSIC), Serrano 144, 28006 Madrid, Spain*
[4]*Instituto de Quimica Física Rocasolano, CSIC, Serrano 119, 28006 Madrid, Spain*

(Received 12 April 2000; revised manuscript received 4 August 2000; published 19 December 2000)

Bragg resonances involving strong interactions among Fourier wave components of a periodically drilled bottom and parametrically driven surface waves on a shallow liquid are experimentally shown to break down the secular dispersion relation of surface waves. When the fluid is sufficiently shallow, wave components that match reciprocal wave vectors of the bottom topography are dominant. Experimental evidence of band-gap phenomena in these surface waves are also shown. Moreover, the prevalence of Bragg resonances is so strong that one of them is excited anomalously within the band gap.

DOI: 10.1103/PhysRevE.63.011204 PACS number(s): 47.35.+i, 47.20.−k, 47.54.+r, 68.05.−n

I. INTRODUCTION

Surface wave propagation on a shallow inviscid liquid in a vessel of variable depth is a classical hydrodynamic problem [1,2]. If the bottom topography is periodic, Bragg resonances can generate strong scattered waves [3]. When the undulations of the periodic bathymetry have large relative amplitudes and/or large slopes, nonlinearities appear and the so-called mild slope equation must be modified [4]. In such a case, a variety of generalized high-order Bragg resonances can be observed [5,6]. Powerful ideas from solid-state physics have also been elegantly used to study the band structure of liquid surface waves [7] and the existence of band-gap phenomena has been theoretically predicted [8]. Furthermore, an experiment of visualization of parametrically driven surface waves over a periodically drilled bottom has been reported recently [9]. In this paper, we present experimental findings based on strong interactions among surface and bottom wave components. Such findings might be useful for the study of other physical systems, in which the strong acousto-optical [10] or optical [11] structural coupling of waves plays a major role. Current experiments of robust visualization of parametrically driven surface waves open a broad scenario to study the propagation of waves in inhomogeneous structures, because they allow the observation of frequency versus wave-number dispersion relations. Localization and band-gap phenomena have been directly observed in elastic waves [12] and, are observed in hydrodynamic systems here.

II. EXPERIMENT

Experiments were made in a transparent vessel, whose bottom consisting of a square lattice of cylindrical wells. The vessel bottom was covered with a shallow layer of a special liquid [13] and was forced to vibrate vertically by means of an exciter coupled to a rod attached to the edge of the box. Moreover, the vessel was covered with a methacrylate lid to prevent evaporation of the liquid. The liquid meniscus at the walls gives rise to a surface wave at the angular frequency ω of the vertical vibration [9,14,15]. To ensure that we only worked with such meniscus waves, vibration amplitudes of the vessel were kept balanced just below the Faraday instability threshold corresponding to the shallow liquid layer among holes [9,14,15].

Wave patterns were obtained by illuminating the bottom of the transparent vessel with optic-fiber-guided white light. Images are focused by the undulating liquid itself at a length s_f from the liquid surface, where a translucent paper screen is placed. Wave amplitudes a are approximately given by the expression $a=\lambda^2/[2\pi^2 s_f(n-1)]$, where λ is the wavelength of the surface wave and n is the refraction index of the liquid [13]. Experiments were recorded on video tape for further analysis.

The depth d of the cylindrical dimples is 2 mm and the liquid depth over the cylindrical wells is given by $h_2=h_1+d$, where the crucial parameter of the experiment is the depth h_1 of the thin liquid layer covering the bottom of the vessel among holes. The liquid was carefully dispensed by means of a measuring pipette and this allows the estimation of depth h_1 by taking into account the covered surface. Experiments were performed for two values of h_1 of about 0.5 and 0.2 mm.

The drilled area fraction f is given by $f=\pi r_0^2/l^2$, where r_0 is the radius of the cylindrical wells and l is the lattice parameter. Experiments for visualization of wave patterns were made with a drilled bottom with 81 holes, $r_0=1.75$ mm and $l=7.5$ mm, what results in a drilled area fraction of 0.17. To study band-gap phenomena several drilled bottom patterns were tested and a square arrangement of 196 cylindrical wells with $r_0=0.75$ mm and $l=2.5$ mm was chosen. Such a pattern only partially covered the middle bottom region of the square vessel and had a drilled area fraction f of about 0.3. Such a value has been experimentally checked as optimum to open larger band gaps.

III. CALCULATION AND VISUALIZATION OF WAVE PATTERNS

Surface wave amplitudes for a wave propagating on a shallow liquid with uniform depth h can be expressed by

$$\eta(\mathbf{r},t)=e^{i\omega t}\psi(x,y), \tag{1}$$

where ω is the angular frequency of the wave and the wave amplitude ψ fulfills the Helmholtz wave equation expressed as

$$\left(\nabla^2+\frac{\omega^2}{c^2}\right)\psi=0, \tag{2}$$

where $c=\omega/k$ is the phase velocity and $k=2\pi/\lambda$ is the wave number, the wavelength being $\lambda \gg h$. Moreover, the angular frequency ω and the wave number k are related by the dispersion relation for inviscid liquids, namely

$$\omega^2=gk\left(1+\frac{T}{\rho g}k^2\right)\tanh(kh), \tag{3}$$

where g is the acceleration due to gravity, T is the liquid surface tension, and ρ is the liquid density [9,14,15].

In the present experiment with periodic bottom topography, when h_1 is about 0.5 mm, wave patterns can be interpreted in the light of standard wave propagation theory in periodic structures, if we assume a perturbation of the wave that propagates over the homogenous bottom. Such a perturbation is introduced by the change of the phase velocity of the wave that propagates over the dimples [16]. To show such a feature, we have built a cellular automaton to solve a system of Helmholtz wave equations over a periodic field. Such a field has two slightly different phase velocities, $c_1=\omega/k_1$ on the host background and $c_2=\omega/k_2$ on the wells, which are calculated according to Eq. (3), for the two depths h_1 and h_2. Such equations are

$$\left(\nabla^2+\frac{\omega^2}{c_i^2}\right)\psi=0, \quad i=1,2, \tag{4}$$

where $c_1<c_2$. Notice that Eq. (4) does not include the $\nabla(c^2)\nabla(\eta)$ term, which Eq. (8) (see below) does. Equation (8) is expected to be more accurate when k is not negligible compared to reciprocal wave-vector magnitudes G of the periodic bottom. From Eq. (3), we see that for shallower and shallower h, and a fixed frequency ω, k increases. Therefore, we must expect that Eq. (4) becomes more accurate, justifying its use for sufficiently shallow depths.

The cellular automaton consists of a discrete square mesh of 20×20 tiny square cells, which mimics the unit cell of the periodic drilled bottom. The Laplace operator is discretized as a first-neighbor increment mean value according to the expression

$$\nabla^2\psi_{i,j}=\frac{1}{4}(\psi_{i-1,j}+\psi_{i,j+1}+\psi_{i+1,j}+\psi_{i,j-1}-4\psi_{i,j}). \tag{5}$$

Periodic boundary conditions are imposed on the sides of the unit cell and the maximum value of ψ is normalized at each iteration. Calculations start with a seed with the shape of a discretized standing plane wave along the [110] direction. Then such a wave is disturbed by successive iterations of the automaton, so that the wave pattern is finally obtained.

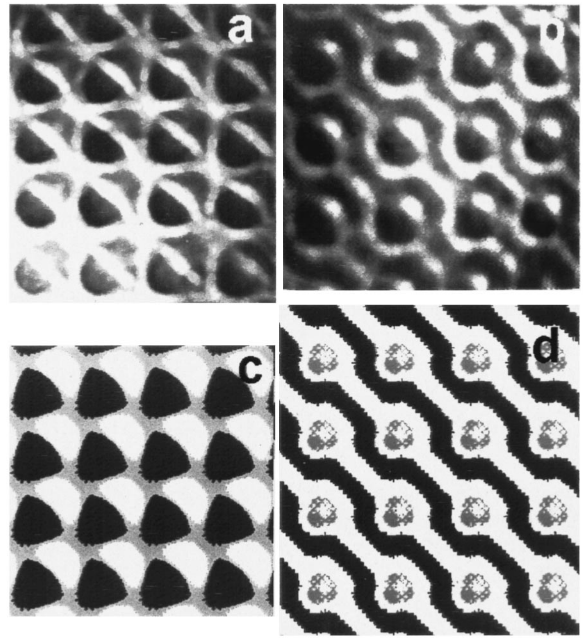

FIG. 1. Wave patterns observed when the liquid depth h_1 is about 0.5 mm at an excitation frequency of (a) 22 Hz and (b) 30 Hz, along with corresponding calculated patterns after (c) 16 and (d) 7 iterations. The lattice parameter l is 7.5 mm.

The drilled area fraction f is 0.17 and the phase velocity ratio c_2/c_1 is 1.42. Two simulated wave patterns are shown in Fig. 1 after 16 and 7 iterations starting from diagonal wave seeds with wavelengths of $l\sqrt{2}/4$ and $7l\sqrt{2}/40$ length units, respectively. As shown in Fig. 1, calculated patterns agree with experimental wave patterns with similarly drilled area fractions and at excitation frequencies of 22 and 30 Hz respectively.

In the present numerical calculation, the phase velocities c_i vary in space periodically between two constants. Therefore, the coupling of waves with the reciprocal wave vectors $\mathbf{G}$ of the periodic bottom is partly included in the model.

Nevertheless, anomalous wave patterns appear when the liquid depth h_1 is as thin as 0.2 mm, and they cannot be simulated with the method mentioned above. Two such patterns are shown in Fig. 2. High-order Bragg resonances involving stronger interactions among bottom and surface wave components seem essential to understand experimental observations under conditions of severe shallow regime.

The Fourier wave development of the square periodic arrangement of cylindrical wells is

$$h(\mathbf{r})=\sum_{\mathbf{G}} A_G e^{i\mathbf{G}\cdot\mathbf{r}}, \tag{6}$$

where $h(\mathbf{r})$ is the function which defines the bottom topography and $\mathbf{G}=(G_x,G_y)=(2\pi p/l,2\pi q/l)$. p and q integers, are the vectors of the reciprocal lattice. Amplitudes A_G are given by

$$|A_{\mathbf{G}}|=\frac{1}{l^2}\int_{\text{unit cell}} d^2\mathbf{r}h(\mathbf{r})e^{-i\mathbf{G}\cdot\mathbf{r}}=2fd\frac{J_1(Gr_0)}{Gr_0}=dF(\mathbf{G}), \tag{7}$$

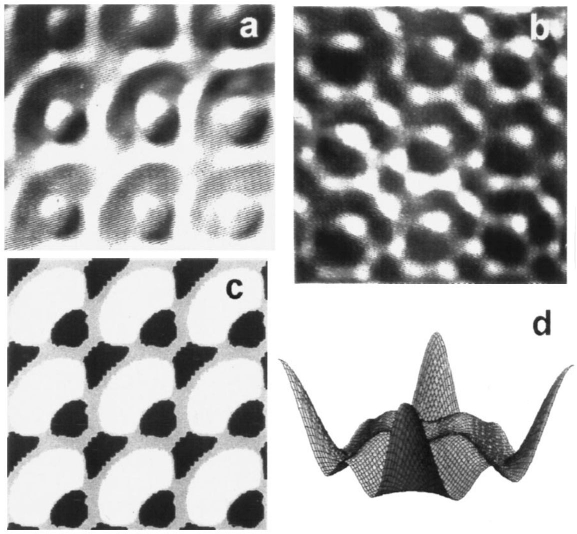

FIG. 2. Wave patterns observed when the liquid depth h_1 is about 0.2 mm at excitation frequencies of (a) 22 Hz and (b) 35 Hz. Modified calculated pattern of (a) is shown in (c). Free-surface wave function of (b) is shown in (d) for a unit cell. The lattice parameter l is 7.5 mm.

where J_1 is the Bessel function of the first kind and order one and $F(\mathbf{G})$ is the structure factor.

Geometric bottom wave vectors $\mathbf{G}$ with integer components in the reciprocal space become resonant with surface wave vectors $\mathbf{k}$. So, the anomalous experimental wave pattern at an excitation frequency of 22 Hz shown in Fig. 2(a) can be calculated now by means of the cellular automaton by taking into account the control of the Bragg resonance. Each iteration is reinforced then by heuristically introducing growing surface waves with wave vectors $\mathbf{k}$ corresponding to the resonance:

$$\mathbf{G}_{(0,1)}+\mathbf{G}_{(1,1)}+\mathbf{G}_{(1,0)}+\mathbf{G}_{(1,-1)}+\mathbf{k}_{(0,-1)}+\mathbf{k}_{(-1,-1)} +\mathbf{k}_{(-1,0)}+\mathbf{k}_{(-1,1)}=0,$$

where surface wave vectors $\mathbf{k}$ have opposite components to the corresponding geometric bottom wave vectors $\mathbf{G}$ defined above. The modified wave pattern is shown in Fig. 2(c), and agrees with the experimental one.

On the other hand, the image of the wave pattern at an excitation frequency of 35 Hz shown in Fig. 2(b) has been analyzed and the resulting free-surface wave function is drawn in Fig. 2(d) over the unit cell. This wave function corresponds to a high-order Bragg resonance involving up to eight surface waves with their wave vectors $\mathbf{k}$ opposite to reciprocal vectors: $\mathbf{G}_{(0,2)}$, $\mathbf{G}_{(1,2)}$, $\mathbf{G}_{(1,1)}$, $\mathbf{G}_{(2,1)}$, $\mathbf{G}_{(2,0)}$, $\mathbf{G}_{(2,-1)}$, $\mathbf{G}_{(1,-1)}$, and $\mathbf{G}_{(1,-2)}$.

The distorted dispersion relations ω versus k seem to fit to the most compatible or nearby Bragg resonance and become controlled by it.

An experiment with a slightly tilted vessel was performed to check the existence of both behaviors described above. This would also show the prevalence of the Bragg resonance regime when the phase velocity ratio is high. When the vessel is tilted, the depth ratio h_2/h_1 and the corresponding phase velocity ratio c_2/c_1 vary continuously, so that both parameters become higher in the region where the liquid depth h_1 is lower. When the depth ratio reaches certain threshold values, the surface wave pattern changes its regime abruptly. This behavior is shown in Fig. 3.

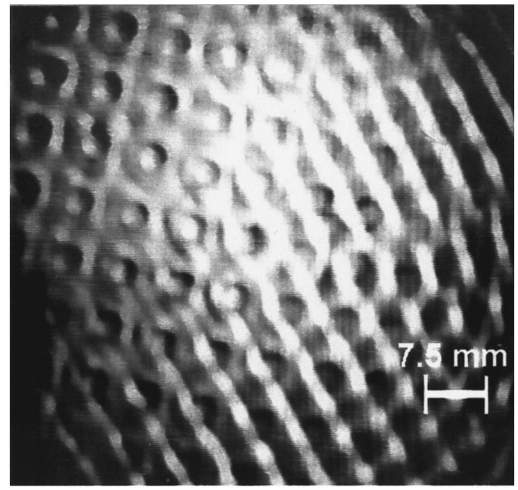

FIG. 3. Complex wave pattern observed on a slightly tilted circular vessel. The vessel is tilted along the diagonal direction defined from top left to bottom right. A clear and well-defined domain appears localized in the shallow enough region, where a conspicuous Bragg resonance is prevalent (top left corner).

IV. CALCULATION AND VISUALIZATION OF BAND-GAP PHENOMENA

In the standard context of band-structure theory, when the wave vector $\mathbf{k}$ of a propagating wave in a periodic structure fulfills the Bragg condition for constructive interference among reflecting waves, $(\mathbf{k}-\mathbf{G})^2=\mathbf{k}^2$, then a frequency band gap $\Delta\omega_g$ appears and the dispersion relation curve, $\omega=\omega(k)$, splits [7,8,16,17]. The main Bragg reflection occurs when $\mathbf{k}$ reaches the boundary of the first Brillouin zone along the [100] direction, i.e., $k=\pi/l$ and $G=2\pi/l$. Then the incident wave is reflected by the periodic structure and the propagating wave decays exponentially. The strengths of both phenomena are proportional to the gap/midgap ratio $\Delta\omega_g/\omega_g$ [17].

To study the band structure and the appearance of band gaps, we use the propagation equation

$$\partial_t^2\eta(\mathbf{r},t)=\nabla[c^2(\mathbf{r})\nabla\eta(\mathbf{r},t)], \tag{8}$$

which is similar to the shallow water equation [1,2,8] and to that used to study acoustic band gaps in two-dimensional periodic systems [18].

By Fourier transforming Eq. (8) and using Bloch's theorem, one obtains the homogeneous equation system

$$\omega^2\eta_{\mathbf{k}+\mathbf{G}}=\sum_{\mathbf{G}'} c^2_{\mathbf{G}-\mathbf{G}'}(\mathbf{k}+\mathbf{G})(\mathbf{k}+\mathbf{G}')\eta_{\mathbf{k}+\mathbf{G}'}, \tag{9}$$

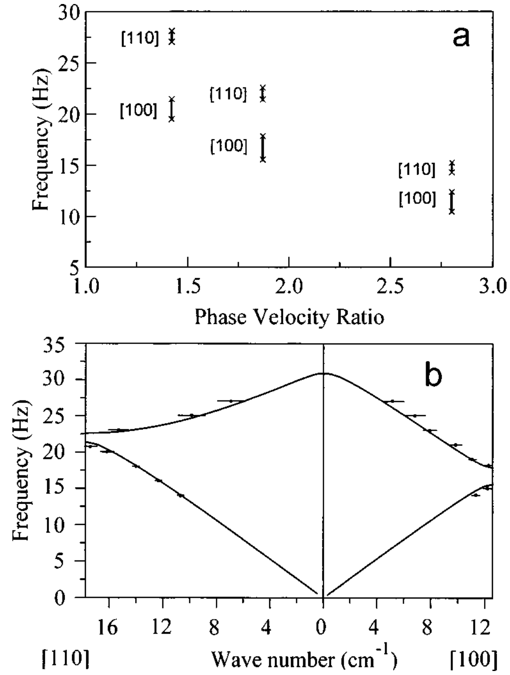

FIG. 4. (a) First band-gap widths along the [100] and [110] directions for three phase velocities ratios. (b) Dispersion relations along [100] and [110] directions with phase velocity ratio of 1.87. Theoretical curves along with experimental results with their corresponding error bars are shown. Amplitudes needed to visualize the wave pattern at frequencies lower than 14 Hz are so high that some holes eject all liquid. On the other hand, the Faraday instability grows for amplitudes of the experiment at frequencies higher than 28 Hz and destroys the propagative wave pattern.

where the Fourier amplitudes $c^2_{\mathbf{G}-\mathbf{G}'}$ are calculated by an expression similar to Eq. (7). The above system has only nontrivial solutions for amplitudes η when the secular equation

$$\det[c^2_{\mathbf{G}-\mathbf{G}'}(\mathbf{k}+\mathbf{G})(\mathbf{k}+\mathbf{G}')-\omega^2\delta_{\mathbf{G},\mathbf{G}'}]=0 \tag{10}$$

is fulfilled. Then amplitudes η are undetermined. In Eq. (10), δ is the Kronecker symbol. Such secular Eq. (10) links angular frequencies ω to wave vectors $\mathbf{k}$ that define the band structure. Calculations in Eq. (10) have been carried out using 12 reciprocal vectors $\mathbf{G}$.

Calculated first band gaps along [100] and [110] directions are shown in Fig. 4(a) for three phase velocity ratios c_2/c_1: 1.42, 1.87, and 2.8. The first two velocity ratios correspond to depths h_1 of about 0.5 and 0.2 mm, respectively, whereas the third one corresponds to an extreme case not studied experimentally. Anyway, no complete band gaps were found, as stated previously [8].

The gap-midgap ratio for the lowest velocity ratio, can be approximately calculated as the first order of perturbation of Eq. (4) as it was studied earlier [16]. Such ratio is given by

$$\frac{\Delta\omega_g}{\omega_g}=c_0^2\left(\frac{1}{c_1^2}-\frac{1}{c_2^2}\right)F(\mathbf{G}), \tag{11}$$

where

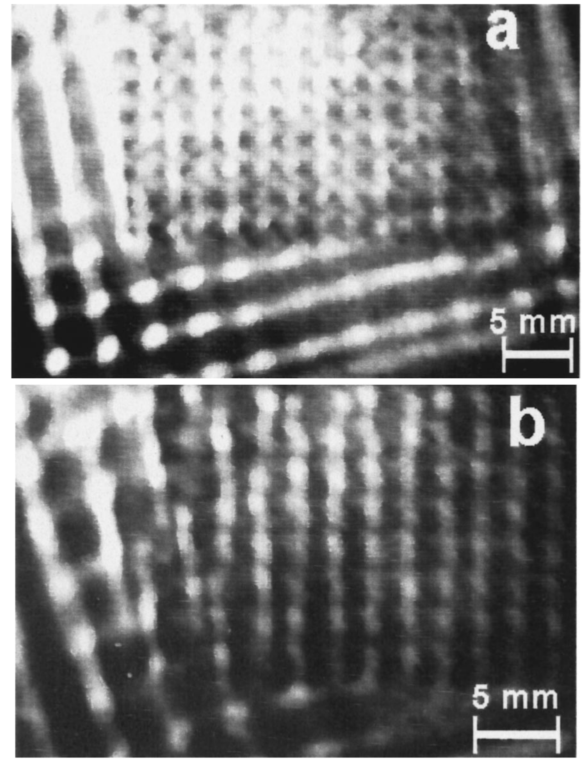

FIG. 5. Visualization of band-gap phenomena when the outer wave that propagates over a flat bottom reaches the periodic bottom region at an angle of (a) 15° and (b) 26°. A slight penetration of the wave into the periodic region can be observed in (b) (top left).

$$\frac{1}{c_0^2}=\frac{f}{c_2^2}+\frac{1-f}{c_1^2}. \tag{12}$$

As it was expected, such an approximation matches with more accurate calculations described by Eq. (10) only for the lowest phase velocity ratio.

Robust band gaps can be easily observed for the phase velocity ratio c_2/c_1 of 1.87. Then the first-order perturbation approximation becomes unrealistic and the band structure must be studied by using Eq. (10). To study the band structure experimentally, we use a partially drilled bottom with a drilled area fraction f of 0.3, as indicated in Sec. II. Calculated and measured dispersion relations for the first two bands of the propagative wave are shown in Fig. 4(b), in which 42 vectors $\mathbf{k}$ have been used to calculate each band.

The band-gap visualization is shown in Fig. 5, where the vessel walls are at an angle ranging from 15° to 26° with respect to the periodic bottom structure. The pattern for an angle of about 15° is shown in Fig. 5(a) at an excitation frequency of 16 Hz, and then calculated and measured band gaps agree within an error lower than 0.5 Hz. When the angle is about 26°, as it is shown in Fig. 5(b), the gap/midgap ratio decreases and the midgap increases, so the outer propagating wave penetrates slightly into the periodic bottom region, as it can be seen on the left side of Fig. 5(b).

Experimental points at the edges of the band gaps correspond to standing waves on the whole drilled bottom region. So, the group velocity of such waves is zero, what corresponds to a zero slope of the dispersion relation curve. No wave that covers the whole drilled region can be observed within the band gaps. Such features allow to determine where the dispersion relation is broken down by the band gap.

The amplitude a of standing waves at the edges of the first band gap is estimated to be about 0.08 mm, what is comparable to depth h_1. On the other hand, the wavelengths for the states at the edges of the band gaps are about 5 and 3.5 mm and the depth h_1 corresponding to the very thin layer of liquid among holes is about 0.2 mm. Then one obtains 0.25 and 0.36, respectively, for kh. This is compatible with the shallow water approximation in which $kh \ll 1$. The surface area among holes takes 70% of the total surface area, so that Eq. (8) works adequately. Indeed, this is confirmed by the good agreement between theory and experimental observations. Anyway, the fitting is better in the first band, for frequencies lower than the band gap, where the group velocity is approximately constant, as it can be seen in Fig. 4(b). This feature indicates a low dispersion of the wave that improves the approximation to the shallow water regime in the first band.

Nevertheless, the main feature in the snapshot shown in Fig. 5 is the prevalent Bragg resonance controlled by the condition $\mathbf{G}_{(0,1)}+\mathbf{G}_{(1,0)}+\mathbf{k}_{(0,-1)}+\mathbf{k}_{(-1,0)}=0$, which is patent over the periodic bottom region. Two dominant perpendicular waves with the same orientation and wavelength as the periodic bottom topography run on the free surface at excitation frequencies within the band gap. Such waves show no dependence on the propagation direction of the external wave. On the other hand, the phases of surface waves on wells remain the same.

Finally, the pattern observed in Fig. 3 is another good example of visualization of the second band gap along the [110] direction and has the same coupling $\mathbf{G}-\mathbf{k}$ mentioned above.

V. CONCLUSIONS

Parametrically driven wave patterns and band-gap phenomena on a shallow fluid covering a periodically drilled bottom have been studied. Experimental wave patterns have been interpreted assuming a model of propagation where the phase velocities vary in space periodically between two constants. When the wave vector reaches the boundary of the first Brillouin zone, wide band gaps break down the dispersion relation curve. For sufficiently shallow fluids, such band-gap phenomena are so robust that they can be directly visualized.

ACKNOWLEDGMENTS

This work has been supported by DGICYT Project No. PB97-1232. We thank Professor N. García and Professor M. M. Sigalas for discussions.

[1] H. Lamb, *Hydrodynamics* (Cambridge University Press, Cambridge, 1995), p. 291.

[2] J. Miles, J. Fluid Mech. **152**, 379 (1985).

[3] A. G. Davies and A. D. Heathershaw, J. Fluid Mech. **144**, 419 (1984); C. C. Mei *ibid.* **152**, 315 (1985); J. T. Kirby, *ibid.* **162**, 171 (1986); C. C. Mei, T. Hara, and M. Naciri, *ibid.* **186**, 147 (1988); M. Naciri and C. C. Mei, *ibid.* **192**, 51 (1988).

[4] P. G. Chamberlain and D. Porter, J. Fluid Mech. **291**, 393 (1995); J. W. Miles and P. G. Chamberlain, *ibid.* **361**, 175 (1998); J. Miles, *ibid.* **376**, 53 (1998); Y. Agnon, Phys. Rev. E **59**, R1319 (1999).

[5] E. Guazzelli, V. Rey, and M. Belzons, J. Fluid Mech. **245**, 301 (1992).

[6] Y. Liu and D. K. P. Yue, J. Fluid Mech. **356**, 297 (1998).

[7] T. Chou, Phys. Rev. Lett. **79**, 4802 (1997).

[8] T. Chou, J. Fluid Mech. **369**, 333 (1998).

[9] M. Torres, J. P. Adrados, and F. R. Montero de Espinosa, Nature (London) **398**, 114 (1999).

[10] Y. Lu, Y. Zhu, Y. Chen, S. Zhu, N. Ming, and Y. Feng, Science **284**, 1822 (1999).

[11] T. Opatrný, B. A. Malomed, and G. Kurizki, Phys. Rev. E **60**, 6137 (1999); V. N. Astratov *et al.*, Phys. Rev. B **60**, R16 255 (1999).

[12] M. Torres, F. R. Montero de Espinosa, D. García-Pablos, and N. García, Phys. Rev. Lett. **82**, 3054 (1999); D. García-Pablos, M. Sigalas, F. R. Montero de Espinosa, M. Torres, M. Kafesaki, and N. García, *ibid.* **84**, 4349 (2000).

[13] The liquid used is Fluorinert FC-75 of the 3M Company, a fully fluorinated organic liquid with low kinematic viscosity $\upsilon = 0.8\times10^{-2}$ cm^2/s, lower than that of the water, very low surface tension $T = 15$ dyn/cm, very high density $\rho = 1.77$ g/cm^3 and refraction index $n = 1.276$.

[14] S. Douady, J. Fluid Mech. **221**, 383 (1990); M. C. Cross and P. C. Hohenberg, Rev. Mod. Phys. **65**, 851 (1993).

[15] M. Torres, G. Pastor, I. Jiménez, and F. Montero de Espinosa, Chaos, Solitons Fractals **5**, 2089 (1995).

[16] L. Brillouin, *Wave Propagation in Periodic Structures* (McGraw-Hill, New York, 1946), Chap. VI.

[17] C. Kittel, *Introduction to Solid State Physics* (Wiley, New York, 1976), Chap. 2, 7, and 9; N. W. Ashcroft and N. D. Mermin, *Solid State Physics* (Saunders, Philadelphia, 1976), Chap. 5, 6, 8, and 9.

[18] M. M. Sigalas, J. Appl. Phys. **84**, 3026 (1998).